CrystEngComm

Accepted Manuscript

This article can be cited before page numbers have been issued, to do this please use: M. N. Ahmed, K. Y. Ansar, S. Aziz, S. Khan, M. N. Tahir, D. M. Gil and A. Frontera, *CrystEngComm*, 2020, DOI: 10.1039/D0CE00335B.

ROYAL SOCIETY OF CHEMISTRY

rsc.li/crystengcomm

Relevant π–hole tetrel bonding interactions in ethyl 2-triazolyl-2-oxo-acetate derivatives: Hirshfeld surface analysis and DFT calculations

Muhammad Naeem Ahmed,[a*] Khawaja Ansar Yasin[a], Shahid Aziz[b], Saba Urooge Khan[c], Muhammad Nawaz Tahir,[d] Diego Mauricio Gil[e] and Antonio Frontera[f*]

[a]*Department of Chemistry, The University of Azad Jammu and Kashmir, Muzaffarabad, 13100 Pakistan*

[b]*Department of Chemistry, Mirpur University of Science and Technology, Mirpur, Azad Kashmir*

[c]*Department of Polymer Engineering and Technology University of The Punjab*

[d]*Department of Physics, University of Sargodha, Sargodha, Pakistan*

[e]*INBIOFAL (CONICET - UNT), Instituto de Química Orgánica - Cátedra de Química Orgánica I, Facultad de Bioquímica, Química y Farmacia, Universidad Nacional de Tucumán, Ayacucho 471 (T4000INI), San Miguel de Tucumán - Tucumán - Argentina*

[f]*Department de Quimica, Universitat de les Illes Balears, Crta. De Valldemossa km 7.5, 07122 Palma de Mallorca (Baleares), Spain*

Abstract: This manuscript reports the synthesis, spectroscopic and X-ray characterization of four triazole derivatives that include an *α*-ketoester functionality and two phenyl substituents. In particular ethyl 2-(4-(4-chlorophenyl)-1-(4-methylbenzyl)-1*H*-1,2,3-triazol-5-yl)-2-oxoacetate (**1**), ethyl 2-(1-(4-methylbenzyl)-4-phenyl-1*H*-1,2,3-triazol-5-yl)-2-oxoacetate (**2**), ethyl 2-(1-benzyl-4-(3-fluorophenyl)-1*H*-1,2,3-triazol-5-yl)-2-oxoacetate (**3**) and ethyl 2-(1-benzyl-4-(4-methoxyphenyl-1*H*-1,2,3-triazol-5-yl)-2-oxoacetate (**4**) were synthesized in good yields. All compounds form self-assembled dimers in the solid state establishing two symmetrically equivalent O···π-hole tetrel bonding interactions. These interactions have been analyzed using Hirshfeld surface analysis, DFT calculations and the Bader's theory of atoms-in-molecules and further rationalized using the molecular electrostatic potential (MEP) surface calculations. We have studied how the nucleophilic/electrophilic nature of the –COOEt and –CO– groups is affected by the substituents of the rings and, consequently, influences the interaction energy of the C···O tetrel bond.

View Article Online
DOI: 10.1039/D0CE00335B

1. Introduction

In the short period click chemistry has had a dramatic and diverse impact in many areas of modern chemistry. The versatility of click chemistry and particularly Cu(I) catalyzed Huisgen cycloaddition seem endless, yet we are still in the early developmental stages of this concept driven research. With the discovery and invention of new chemical transformations which meet click status, the future looks bright for click chemistry[1].

1,4,5-Trisubstituted 1,2,3-triazoles have been regarded as highly significant nitrogen-containing heterocycles due to their broad spectrum of biological activities and other prominent properties[2]. 1,2,3-Triazole scaffolds are ubiquitous structural motifs in various bioactive molecules, pharmaceutical agents and functional materials. Therefore, they have been used in several fields ranging from medicinal chemistry to materials science[3]. Furthermore, 1,2,3-triazoles have also been investigated as powerful and versatile ligands for metal coordination, exhibiting tremendous application prospects[4].

In addition to the ubiquitous H-bond, [5-8] σ-hole-based[9, 10] noncovalent interactions are also relevant in many areas of chemistry, like crystal engineering[11-13] and catalysis. The σ-hole can be defined as a region of positive potential in a main group element located opposite to a covalent bond[14, 15]. Similarly, some molecules also exhibit π-holes which lie usually above and below the plane of the system[16-20], leading to π-hole interactions with Lewis bases[10]. In X-ray structures, π-hole interactions were identified by Bürgi and Dunitz in 1975[19], thus revealing the trajectory along which a nucleophile attacks the π-hole of carbonyl group. Moreover, the relevance of n → π* interactions in proteins from a lone pair of electrons (n) to the antibonding orbital (pi*) of carbonyl group has been demonstrated[21]. In addition, significant π-hole interaction have been described an studied in benzoic acid dimers[22], nitro derivatives[23-27], and acyl carbon containing molecules[28-30]. The physical nature and factors affecting the strength of π-hole interactions are similar to those of σ-hole interactions[30].

In continuation of our previous work highlighting the importance of antiparallel π–π interactions[31] here in this manuscript we report the synthesis and X-ray characterization of four 1,4,5-trisubstituted 1,2,3-triazoles (Scheme 1) that include an *α*-ketoester functionality[32]. Interestingly, these compounds form self-assembled dimers in the solid state where two symmetrically equivalent O··· π-hole interactions are established. These interactions have been analyzed using Hirshfeld surface analysis, DFT calculations and

View Article Online
DOI: 10.1039/D0CE00335B

the Bader's theory of atoms-in-molecules and rationalized using the molecular electrostatic potential (MEP) surface calculations.

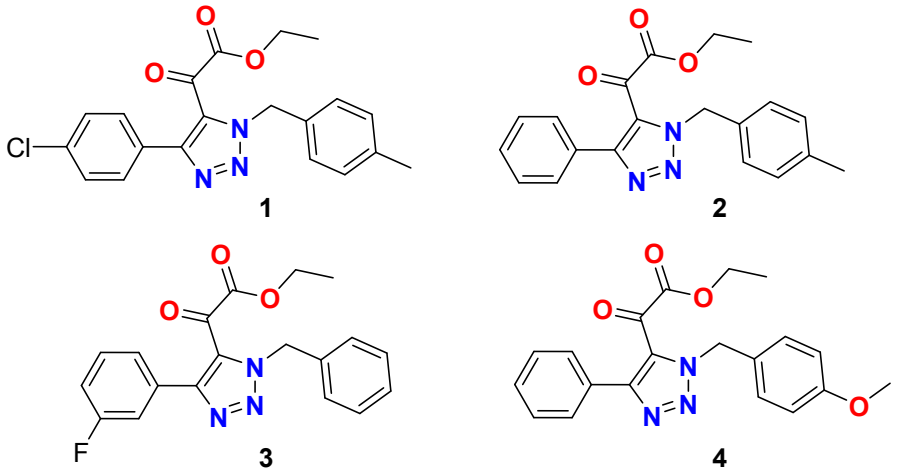

Scheme 1 1,4,5-Trisubstituted 1,2,3-triazoles (**1-4**)

2. Experimental and theoretical methods

2.1. Synthesis

Compounds **1-4** were synthesized by following a procedure already published by us[32, 33] and were mainly characterized by UV, IR (Fig. 1), HRMS and single crystal X-ray crystallography. Melting points were determined on a Yanaco melting point apparatus and are reported as uncorrected. FT-IR spectra were recorded on SHIMADZU FTIR-8400S spectrophotometer using KBr disc method. Similarly, double beam SHIMADZU UV-1601 UV-visible spectrophotometer was used to scan UV.^{1}H-NMR (300 MHz) and ^{13}C-NMR (100 MHz) spectra were measured on a JEOL-ECA instrument in DMSO and TMS as internal standard.

2.1.1. Ethyl 2-(4-(4-chlorophenyl)-1-(4-methylbenzyl)-1H-1,2,3-triazol-5-yl)-2-oxoacetate (1)

White crystalline solid, m. p. 100-102°C , Yield = 83%, R_f = 0.5(*n*-hexane:EtOAc), λ_{max} = 311.74 nm in EtOH(0.01g/L); IR (KBr, cm^{-1}): ν_{max} 3084($CH_{arom.}$), 1743 (CO), 1678 (C=C), 1480 (CH_2 rocking); ^{1}H-NMR δ ppm 7.50-7.14 (m, 8H), 5.83 (s, 2H), 3.84 (q, 2H, *J* = 7.2 Hz), 2.32 (s, 3H), 1.01 (t, 3H, *J* = 7.2 Hz); ^{13}C-NMR δ ppm 177.1, 160.8,151.6,138.6, 136.0,131.1, 130.3, 129.5, 128.9, 128.2, 127.1, 63.0, 54.1, 21.1, 13.4. HRMS (ESI-TOF) (m/z): calculated for $C_{20}H_{18}ClN_3O_3$, $[M+H]^+$ 384.1109; observed 384.1103.

2.1.2.*Ethyl 2-(1-(4-methylbenzyl)-4-phenyl-1H-1,2,3-triazol-5-yl)-2-oxoacetate (2)*

White crystalline solid, m. p. 83-85°C, Yield = 92%, R_f = 0.6(*n*-hexane:EtOAc), λ_{max} = 303.37 nm in EtOH (0.01g/L); IR (KBr, cm^{-1}): ν_{max} 3057($CH_{arom.}$), 1739 (CO), 1682 (C=C), 1449 (CH_2 rocking); ^{1}H-NMR δ ppm 7.51-7.14 (m, 9H), 5.85 (s, 2H), 3.74 (q, 2H, *J* = 7.2 Hz), 2.32 (s, 3H), 0.93 (t, 3H, *J* = 7.2 Hz); ^{13}C-NMR δ ppm 177.4, 160.9,152.9,138.5, 134.9,131.3, 129.7, 129.4, 129.0, 128.6, 128.2, 127.1,62.8, 54.0, 21.1, 13.2.HRMS (ESI-TOF) (m/z): calculated for $C_{20}H_{19}N_3O_3$, $[M+H]^+$ 350.1499; observed 350.1502.

2.1.3. *Ethyl 2-(1-benzyl-4-(3-fluorophenyl)-1H-1,2,3-triazol-5-yl)-2-oxoacetate (3)*

White crystalline solid, m. p. 66-68°C, Yield = 22%, R_f = 0.5(*n*-hexane:EtOAc), λ_{max} = 256.52, 313.80 nm in EtOH(0.01g/L); IR (KBr, cm^{-1}): ν_{max} 3063 ($CH_{arom.}$), 1739 (CO), 1689 (C=C), 1483 (CH_2 rocking); ^{1}H-NMR δ ppm 7.46-7.13 (m, 9H), 5.88 (s, 2H), 3.85 (q, 2H, *J* = 7.2 Hz), 1.03 (t, 3H, *J* = 7.2 Hz); ^{13}C-NMR δ ppm 177.1, 162.6 (d, J_{CF} = 245.9 Hz), 160.7, 151.4, 134.1,131.7(d, J_{CF} = 7.89 Hz) 130.4(d, J_{CF} = 8.60 Hz), 128.8, 128.7, 128.2, 127.5, 124.9, 116.8 (d, J_{CF} = 20.8 Hz), 115.9 (d, J_{CF} = 22.9 Hz), 63.0, 54.3, 13.3. HRMS (ESI-TOF) (m/z): calculated for $C_{19}H_{16}FN_3O_3$, $[M+H]^+$ 354.1248; observed 354.1244.

2.1.3. *Ethyl 2-(1-benzyl-4-(4-methoxyphenyl-1H-1,2,3-triazol-5-yl)-2-oxoacetate (4)*

White crystalline solid, m. p. 128-130°C, Yield = 78%, R_f = 0.5(*n*-hexane:EtOAc), λ_{max} = 332.58 nm in EtOH(0.01g/L); IR (KBr, cm^{-1}): ν_{max} 3066 ($CH_{arom.}$), 1744 (CO), 1672 (C=C), 1450 (CH_2 rocking); ^{1}H-NMR δ ppm 7.46-6.97 (m, 9H), 5.88 (s, 2H), 3.79 (q, 2H, *J* = 7.2 Hz), 2.82 (s, 3H), 0.99 (t, 3H, *J* = 7.2 Hz); ^{13}C-NMR δ ppm 177.4, 161.1, 160.8, 152.8, 134.3, 130.4, 128.8, 128.5, 128.1, 126.9, 122.0, 114.1, 62.8, 55.3, 54.2,13.3. HRMS (ESI-TOF) (m/z): calculated for $C_{20}H_{19}N_3O_4$, $[M+H]^+$ 366.1448; observed 366.1445.

View Article Online
DOI: 10.1039/D0CE00335B

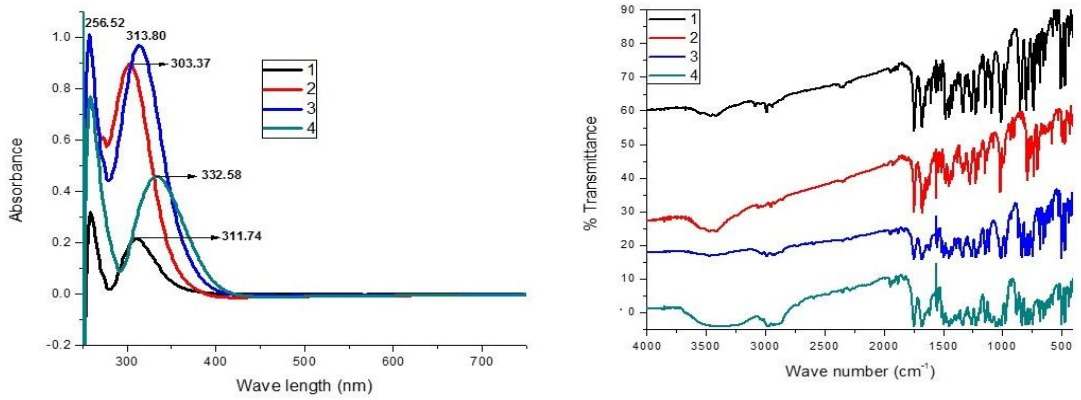

Fig. 1 UV(left) in EtOH and IR (right) spectra of compounds (**1-4**)

2.2 Crystallization conditions

Some good-quality single crystals of compounds **(1-4)** suitable for X-ray diffraction analysis were grown from a mixture of EtOH and EtOAc (dissolving 150 mg of each compound in 5 ml of solvent) by slow evaporation over a period of 48h at room temperature.

2.3 X-ray data collection and structure refinement

Suitable single crystals of compounds **1-4** were selected for X-ray analyses and diffraction data were collected on a Bruker Kappa APEX-II CCD detector with MoKα radiations at 100 K. Using the SADABS program semi emperical correction was applied[34]. SHELX program was also used to solve all structures by direct method[35].Positions and anisotropic parameters of all non-H atoms were refined on F^2 using the full matrix least-squares technique. The H atoms were added at geometrically calculated positions and refined using the riding model[36].The details of crystallographic data and crystal refinement parameters for the compounds **1-4** are given in Table 1.

Table: 1 Crystallographic data and details of refinements for compounds 1-4

	1	**2**	**3**	**4**
CCDC	988864	988860	988859	988858
Chemical formula	$C_{20}H_{18}ClN_3O_3$	$C_{20}H_{19}N_3O_3$	$C_{19}H_{16}FN_3O_3$	$C_{20}H_{19}N_3O_4$
M_r	383.82	349.38	353.35	365.38
Crystal system, space group	Triclinic, $P\bar{1}$	Monoclinic, $P2_1/c$	Monoclinic, $C2/c$	Triclinic, $P\bar{1}$

View Article Online
DOI: 10.1039/D0CE00335B

Temperature (K)	296	296	296	296
a, *b*, *c* (Å)	8.3157 (6), 9.5082 (8), 13.1245 (10)	8.2517 (3), 17.9945 (9), 12.2748 (6)	28.5939 (14), 7.5267 (4), 19.3890 (8)	8.2922 (6), 9.4246 (7), 12.9343 (10)
α, β, γ (°)	68.898 (4), 86.538 (4), 85.332 (4)	99.877 (2)	121.964 (1)	111.004 (2), 99.018 (3), 97.623 (2)
V (Å^3)	964.38 (13)	1795.61 (14)	3540.2 (3)	912.24 (12)
Z	2	4	8	2
Radiation type	Mo *K*α	Mo *K*α	Mo *K*α	Mo *K*α
μ (mm^{-1})	0.22	0.09	0.10	0.09
Crystal size (mm)	0.38 × 0.32 × 0.30	0.40 × 0.30 × 0.28	0.38 × 0.28 × 0.25	0.36 × 0.30 × 0.25
Diffractometer	Bruker Kappa APEXII CCD	Bruker Kappa APEXII CCD	Bruker Kappa APEXII CCD	Bruker Kappa APEXII CCD
Absorption correction	Multi-scan (*SADABS*; Bruker, 2005)	Multi-scan (*SADABS*; Bruker, 2005)	Multi-scan (*SADABS*; Bruker, 2005)	Multi-scan (*SADABS*; Bruker, 2005)
T_{min}, T_{max}	0.670, 0.746	0.670, 0.746	0.670, 0.746	0.670, 0.746
No. of measured, independent and observed [$I > 2\sigma(I)$] reflections	13504, 3701, 2645	16244, 4114, 2801	14823, 3806, 2426	14140, 4016, 3299
R_{int}	0.021	0.025	0.034	0.027
$(\sin \theta/\lambda)_{max}$ (Å^{-1})	0.617	0.649	0.638	0.644
$R[F^2 > 2\sigma(F^2)]$, $wR(F^2)$, S	0.057, 0.168, 1.06	0.053, 0.167, 1.04	0.062, 0.217, 1.02	0.046, 0.126, 1.05
No. of reflections	3701	4114	3806	4016
No. of parameters	246	237	267	249
H-atom treatment	H-atom parameters constrained	H-atom parameters constrained	72	4
$\Delta\rangle_{max}$, $\Delta\rangle_{min}$ (e Å^{-3})	0.44, -0.50	0.26, -0.23	0.95, -0.33	0.26, -0.25

Computer programs: *APEX2* (Bruker, 2007), *SAINT* (Bruker, 2007), *SHELXS97* (Sheldrick, 2008), *SHELXL2018*/3 (Sheldrick, 2015), *ORTEP-3 for Windows* (Farrugia, 1997) and *PLATON* (Spek, 2009), *WinGX* (Farrugia, 1999) and *PLATON* (Spek, 2009).

2.4. Computational methods

The calculations of the noncovalent interactions and molecular electrostatic potential (MEP) surfaces were carried out using the Gaussian-16[37] and the PBE1PBE-D3/def2-TZVP level of theory. The ultrafine grid has been used in the calculations to ensure the accuracy of the results. The Grimme's D3 dispersion correction has been used in the calculations[38]. The interaction energies are not BSSE corrected because we have evaluated it in the reduced models of compounds **1-4** and the error is < 4%. To evaluate the interactions in the solid state, the crystallographic coordinates were used and only the position of the H-bonds has been optimized. This procedure and level of theory has been successfully used to evaluate similar interactions[39]. The interaction energies were computed by calculating the difference between the energies of the isolated monomers

View Article Online
DOI: 10.1039/D0CE00335B

and their assembly. The QTAIM calculations[40] have been performed at the same level of theory by means of the AIMAll program.[41]

2.5. Hirshfeld surface calculations

The Hirshfeld surfaces (HS) analysis and their associated two-dimensional fingerprint (FP) plots[42-44] were used to identify and quantify the contribution of different intermolecular interactions existing on the crystal structure and to understand the nature of these interactions. The HS and FP plots were generated using the CrystalExplorer 3.1.[45] The normalized contact distance (d_{norm}) enables the identification of the regions of particular importance to the intermolecular interactions. In this surface, any close intermolecular contact will be characterized by two identical red regions. The Hirshfeld surfaces for the studied structures were also mapped with the *shape index* and *curvedness* properties. The 3D d_{norm} surfaces were mapped over a fixed color scale of -0.075 a.u. (red) to 0.75 a.u. (blue) and *shape index* mapped in the color range of –1.0 a.u. (concave) to 1.0 a.u. (convex) and *curvedness* mapped in the range of –4.0 a.u. (flat) to 4.0 a.u. (singular). A final analysis of the intermolecular interactions and their contribution to the crystal packing was performed by using 2D FP plots. These plots were mapped using the translated 0.6-2.4 Å range including reciprocal contacts.

3. Results and Discussion

3.1 Structural description

In ethyl 2-(4-(4-chlorophenyl)-1-(4-methylbenzyl)-1*H*-1,2,3-triazol-5-yl)-2-oxoacetate (**1**), the 4,5-dihydro-1*H*-1,2,3-triazole group A (C5/C6/N1-N3), the 4-chlorophenyl moiety B (C7-C12/Cl1), the 4-methylbenzyl group C (C13-C20) are planar with r. m. s deviation of 0.0039, 0.0123 and 0.0361 Å, respectively. The dihedral angles A/B, A/C and B/C are 42.09(11)°, 83.32 (8)°and 67.39(6)°, respectively. The molecules are connected with each other in the form of dimers through C-H···O hydrogen bonds (see Fig. 2). In addition, C20-H20B···N1 hydrogen bonds are observed. The crystal structure of **1** shows C-H···π interactions, with Cg1 distance of 2.797 Å (Cg1: C14-C19). The crystal packing appears to be controlled by weak π-stacking interactions [d(Cg1···Cg1) = 4.402 Å] involving both 4-methylphenyl rings.

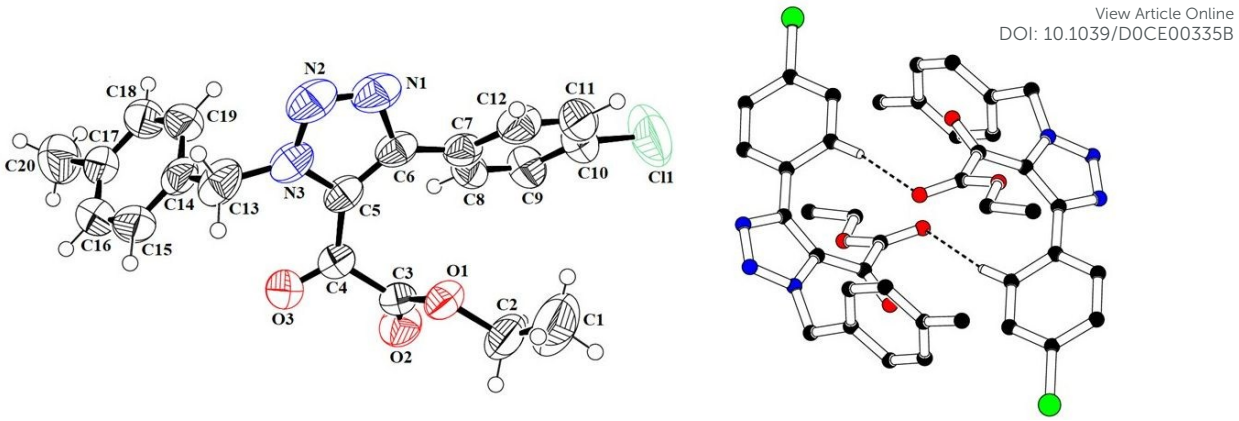

Fig. 2 The ORTEP plot of **1** (left) showing the atom numbering, with displacement ellipsoids at the 50% probability level while **1** (right) indicates that molecules are dimmerized. The H-atoms not involving in H-bonding are omitted for clarity.

In ethyl 2-(1-(4-methylbenzyl)-4-phenyl-1*H*-1,2,3-triazol-5-yl)-2-oxoacetate (**2**), the 4,5-dihydro-1*H*-1,2,3-triazole group A (C5/C6/N1-N3), the phenyl ring B (C7-C12), the 4-methylbenzyl group C (C13-C20) are planar with r. m. s deviation of 0.0048, 0.0023 and 0.0423 Å, respectively. The dihedral angles A/B, A/C and B/C are 47.93(7)°, 74.97(6)°and 27.50(9)°, respectively. The molecules are connected through C-H···O hydrogen bonds between the H atom from the 4-methylbenzyl group and the O-atoms from the keto group (Fig. 3). The supramolecular assembly of **2** also includes π···π stacking interactions between the phenyl (Cg1: C7-C12) and triazole (Cg2: C5/N3/N2/N1/C6) rings with an inter-centroid distance of 3.809 Å.

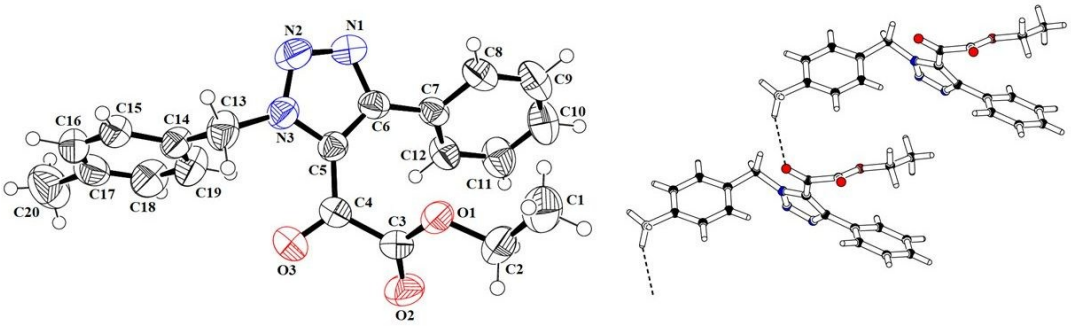

Fig. 3 The ORTEP plot of **2** (left) showing the atom numbering, with displacement ellipsoids at the 50% probability level while **2** (right) indicates the H-bonding packing pattern showing that molecules are interconnected through C(11) chains.

In the ethyl 2-(1-benzyl-4-(3-fluorophenyl)-1H-1,2,3-triazol-5-yl)-2-oxoacetate (**3**), the benzene ring of benzyl group is disordered over two set of sites with occupancy ratio of 0.54(3): 0.46(3). The 4,5-dihydro-1*H*-1,2,3-triazole group A (C5/C6/N1-N3), the 3-flourobenzene moiety B (C7-C12/F1), the benzyl group containing major part of disordered benzene ring C (C13/C14A-C19A) and the benzyl group containing minor part of disordered benzene ring D (C13/C14B-C19B) are planar with r. m. s deviation of 0.0056, 0.0055, 0.0132 and 0.0170 Å, respectively. The dihedral angles A/B, A/C, A/D are 37.34(10)°, 55.19(4)° and 80.59(5)°, respectively. The major part of disordered benzene ring is twisted at an angle of 24.05(1)° with respect to minor part of it. The ethyl 2-oxoacetate group is not planar. In this group, the torsion angles O1-C3-C4-O3 and O2-C3-C4-O3 are -142.0(2)° and 35.7(4)°, respectively. The molecules are connected with each other through C-H···O bonding to form $R_1^2(5)$ loops, where the CH belongs to the fluorobenzene moiety and O-atoms are from the keto groups of the ethyl 2-(4,5-dihydro-1H-1,2,3-triazol-5-yl)-2-oxoacetate part of the molecule. The non-carbonyl oxygen atom is linked to the CH attached to the disordered benzene ring through C-H···O hydrogen bonds. The CH of the disordered benzene ring is also linked with the carbonyl atom that is closer to 4,5-dihydro-1*H*-1,2,3-triazole group as compared to other carbonyl oxygen through C-H···O bonding as given in Table 2 and shown on right side of Fig. 4. In this way, each molecule is linked with three adjacent molecules (Fig. 4).

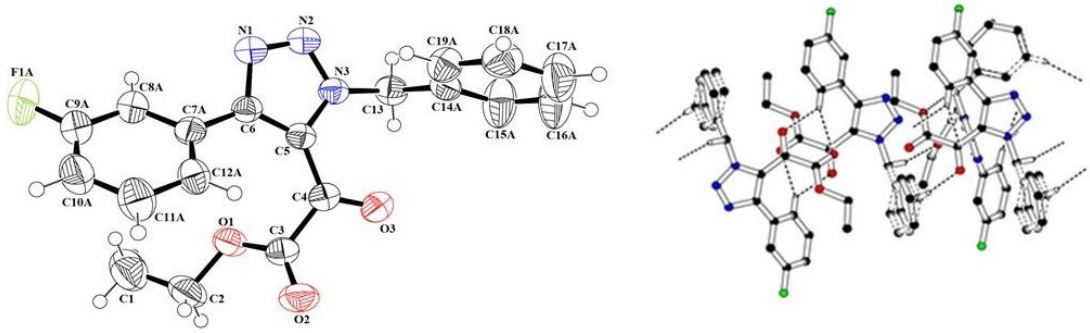

Fig. 4 The ORTEP plot of **3** (left) showing the atom numbering, with displacement ellipsoids at the 50% probability level while **3** (right) indicates the hydrogen bonding pattern. The H-atoms not involved in H-bonding are omitted for clarity.

In the ethyl 2-(1-benzyl-4-(4-methoxyphenyl-1*H*-1,2,3-triazol-5-yl)-2-oxoacetate (**4**), the ethoxalyl group A (C1/C2) is disordered over two set of sites with occupancy ratio 0.719(11): 0.281(11). The ethoxalyl group B (O1/C1A/C2A) containing major part of

View Article Online
DOI: 10.1039/D0CE00335B

disordered CH_3CH_2- moiety and another ethoxalyl group C (O1/C1B/C2B) containing minor part of disordered ethane moiety are planar with a dihedral angle B/C of 45.8 (2)°. The propan-2-ol group D (C3-C5/O3) is planar with r. m. s deviation of 0.0099 Å with dihedral angles B/D, C/D are 48.18 (75)° and 9.48 (2)°, respectively. The 4,5-dihydro-1*H*-1,2,3-triazole group E (C5/C6/N1-N3), the anisole group F (C7-C13/O4) and toluene group G (C14-C20) are planar with r. m. s deviation of 0.0036, 0.0674 and 0.0217 Å, respectively. The dihedral angles D/E, E/F, F/G are 14.1 (1)°, 44.7(6)° and 66.8 (4)°, respectively. The molecules are connected with each other in the form of dimer through C-H···O bonding to form $R_2^2(12)$ loop, where CH is from methyl group of toluene and O-atom is from the 4,5-dihydro-1*H*-1,2,3-triazole-5-ketoester part of the molecule (Fig. 5). The dimers are interlinked through C-H···O hydrogen bonds, their geometric features are given in Table 2.

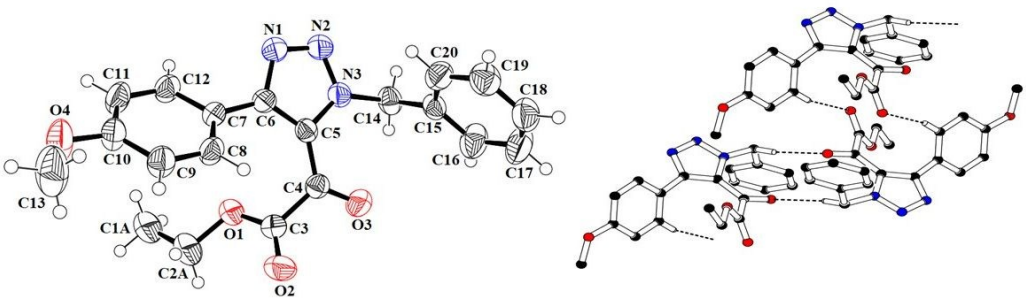

Fig. 5: The ORTEP plot of **4** (left) showing the atom numbering, with displacement ellipsoids at the 50% probability level without the minor part of disordered group while **4** (right) indicates the hydrogen bonding pattern. The H-atoms not involved in H-bonding are omitted for clarity.

Table 2: Hydrogen-bond geometric features with symmetry codes for compounds 1-4.

Compound	*D*—H···*A*	*D*—H	H···*A*	*D*···*A*	*D*—H···*A*
1	C8—H8···O2^{i}(i) −*x*, −*y*+1, −*z*+1.	0.93	2.55	3.448 (3)	163
2	C20—H20*C*···O3^{i}(i) *x-1*, *y*, *z*.	0.96	2.48	3.374 (4)	155
3	C13—H13A···O1^{i}(i) −*x*+1/2, *y*−1/2, −*z*+1/2	0.97	2.52	3.468 (3)	164
	C18*B*—H18*B*···O3^{ii}(ii) *x*, *y*−1, *z*	0.93	2.39	3.284 (10)	161
	C12—H12···O2^{iii}(iii) −*x*+1/2, −*y*+1/2, −*z*+1	0.93	2.54	3.414 (3)	158
	C12—H12···O3^{iii}(iii) −*x*+1/2, −*y*+1/2, −*z*+1	0.93	2.60	3.307 (3)	133
4	C14—H14*B*···O3^{i}(i) −*x*+1, −*y*, −*z*	0.97	2.58	3.542 (2)	173
	C8—H8···O2^{ii}(ii) −*x*+2, −*y*, −*z*	0.93	2.55	3.459 (2)	164

Hirshfeld surface analysis

HS analysis is a useful visualization tool for the analysis of intermolecular interactions in the crystal packing and FP plots are used herein to quantify the contribution of various intermolecular contacts present in the crystal structures of **1-4**. Fig. 6 shows Hirshfeld surfaces mapped over the d_{norm} function in two orientations (columns 1 and 2). Contacts with distances equal to the sum of the vdW radii are represented as white regions and contacts with distances shorter than and longer than vdW radii are represented as red and blue colors, respectively. The full FP plots for compounds **1-4** are displayed in Fig. 7.

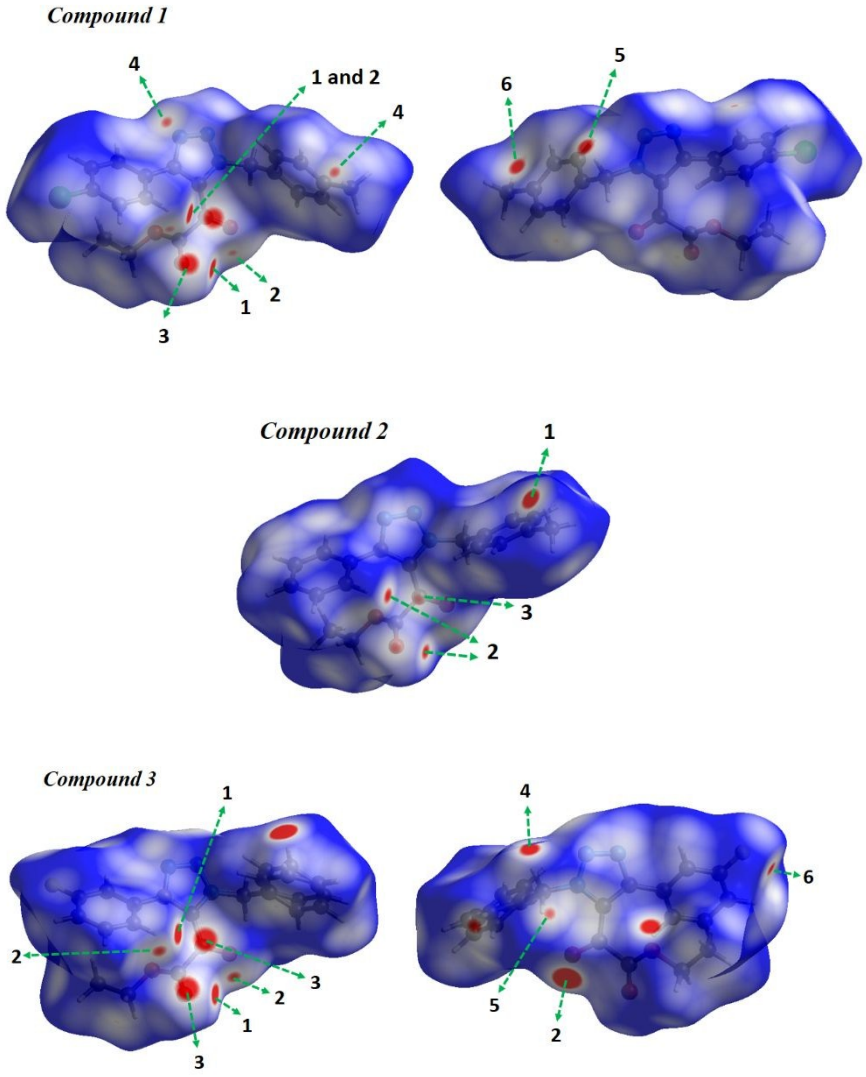

View Article Online
DOI: 10.1039/D0CE00335B

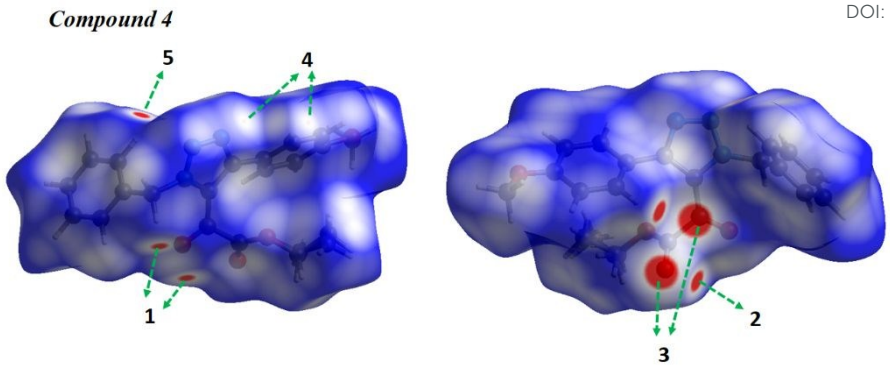

Fig. 6. Views of the Hirshfeld surfaces of compounds **1-4** (columns 1-2) mapped with d_{norm} in two orientations: front view and back view (180° rotated around the vertical axes of the plot). The labels are discussed in the text.

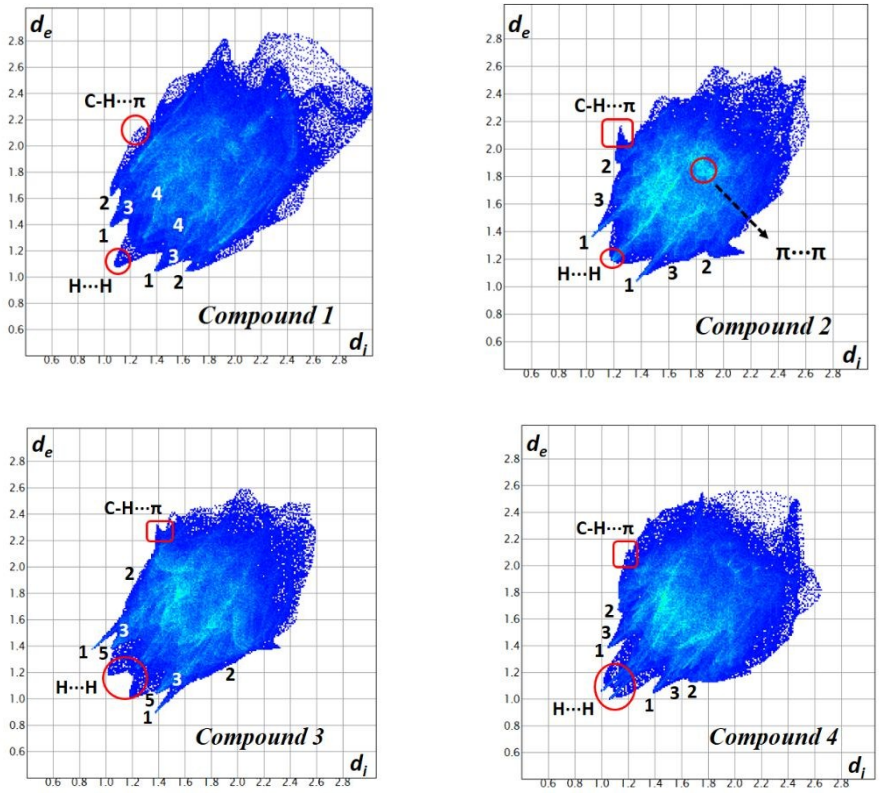

Fig. 7. Full 2D fingerprint plot for compounds **1-4**.

The large regions labelled 1 in Fig. 6, represent H···O/O···H contacts, which are relevant in the d_{norm} maps for all the compounds. These contacts are attributed to C8-H8···O3 and

View Article Online
DOI: 10.1039/D0CE00335B

C8-H8···O2 hydrogen bonds for compound **1** and to C12-H12···O3 and C12-H12···O2 for compound **3**, which can also be seen in the FP plots as a pair of symmetrical spikes at (d_e+d_i) sum of 2.45 Å for the former and at $(d_e+d_i) \sim 2.40$ Å for the later interaction. The H···O/O···H contacts are dominant in compounds **1** and **2** with 12.8 and 16.8 %, respectively, of the total HS area.

The red spot labelled 5 in the d_{norm} map for compound **1** (Fig. 6, column 2) represents H···C/C···H contacts with 17.5% of contribution. In the crystal packing of compound **1**, C-H···π interactions are observed, where the H···C/C···H contacts appear in the form of pronounced "wings" on the sides of the FP plot, a characteristic way for C-H···π interactions. In addition, the supramolecular assemblies of compounds **1** and **2** also include π···π stacking interactions, that are visible in the d_{norm} surface as a red spot labelled 6 in compound **1**. The shape index and curvedness maps (Figure S1 and S2 for compounds **1** and **2**, respectively) are significant indicators for π-stacking interactions. The pairs of complementary red and blue triangles in the *shape index* and large and flat green regions at the side of the molecule in *curvedness* are an indicative of π-stacking interactions.

The red spot labelled 4 in the d_{norm} surface of compound **1** is attributed to C-H···N hydrogen bonds involving the acceptor N1 and one hydrogen atom H20B of the methyl group. The pair of sharp spikes labelled as 3 in the FP plots of compound **1**, are associated to N···H contacts with 11.1% of contribution to the total HS area.

The larger deep-red spots labelled 3 in the d_{norm} surfaces of compounds **1**-**4** are attributed to stronger O2···C4 interactions with a contribution of 2.0% to the total Hirshfeld surface.

The d_{norm} surface of compound **2** shows deep red regions labelled 1 and 2, attributed to C20-H20C···O3 and C12-H12···O2 hydrogen bonds. Like in the structure of compound **1**, the broad spikes at $(d_e+d_i) \sim 3.3$ Å in the FP with 15.1% of contribution to the Hirshfeld surface area, are associated to C-H···π interactions.

In compound **3**, the red regions labelled 4 in the d_{norm} surfaces (Fig. 6) are attributed to C13-H13A···O1 involving the O1 of the carboxylic group as acceptor and the H13A atom of the methylene group linked to the triazole ring. Note that the H13B of the methylene group bounded to the triazole ring is involved in a bifurcated hydrogen bonds C13-

View Article Online
DOI: 10.1039/D0CE00335B

H13B···N1 and C13-H13B···N2 with both N1 and N2 atoms as acceptors. These interactions are observed as spikes labelled 3 in the FP plot (Fig. 7 with a contribution of 9.5% to the total Hirshfeld surface. In addition, the characteristic "wings" at (d_e+d_i) ~ 3.7 Å indicate weak C-H···π interactions involving the H2B atom of the ethyl group and the C18 atom of the phenyl ring. The red spot labelled 6 in the d_{norm} map shows weak H···F/F···H contacts attributed to C15-H15A···F1 hydrogen bonds, which are viewed as a pair of broad spikes labelled 5 in the FP plot with a notable contribution of 10.4% to the Hirshfeld surface area.

In compound **4**, the H···O/O···H contacts labelled 1 in Fig. 6 are again dominant, appearing as two larger deep red spots around the H14B and around the O3 atom attributed to the strongest C14-H14B···O3 hydrogen bonds. These interactions form $R_2^2(12)$ ring motifs. The deep red spot labelled 2 in the d_{norm} surface is associated to C8-H8···O2 hydrogen bonds involving the H8 atom of the aromatic ring and the O2 atom of the carboxylic group. These interactions are observed in the FP plots as symmetric spikes at (d_e+d_i) ~ 2.5 Å and a contribution of 18.0% to the total Hirshfeld surface area. The tiny red regions labelled 4 in the d_{norm} map are attributed to weak C12-H12···N1 hydrogen bonds forming centre-symmetric dimers, giving $R_2^2(10)$ graph-set motifs. The proportion of H···N/N···H interactions comprise 12.2% of the total HS and are characterized by spikes at (d_e+d_i) ~ 2.8 Å in the FP plots. The supramolecular assembly of compound **4** also suggests the existence of C-H···π interactions involving the H19 of the phenyl ring and the C6 atom of the triazole ring. These interactions are visible in the d_{norm} surface as red spots labelled 5, with a contribution of 19.2% to the total HS area.

Theoretical DFT analysis

Experimentally four new triazole derivatives have been synthesized and X-ray characterized (see Figs 2-5). These compounds present different substitution in the aromatic rings. Moreover, the triazole is substituted by an α-ketoester (ethyl-2-oxoacetate) group that is very relevant determining their solid state architecture as it is further commented below.

We have first computed the molecular electrostatic potential (MEP) surfaces of compounds **1**–**4** in order to know the most electrophilic and nucleophilic parts of the molecules and to rationalize the interactions observed in their crystal packing. As a model

compound we show the MEP surface of compound **1** in Fig. 8 and the energetic values for the rest of the complexes in Table 3. It can be observed that the presence of a π-hole (region of positive potential) over the C-atom of the keto group with an associated MEP value of +16.9 kcal/mol. The most negative values are located at the carbonyl O-atom of the ester group and at the O-atom of the keto group. The MEP values are also positive at the aromatic H-atoms, ranging from +14 to +18 kcal/mol. This analysis evidences that the interaction of the electron rich O-atoms with either the C-atom of the keto group or the aromatic H-atoms is equally favored, from an electrostatic point of view.

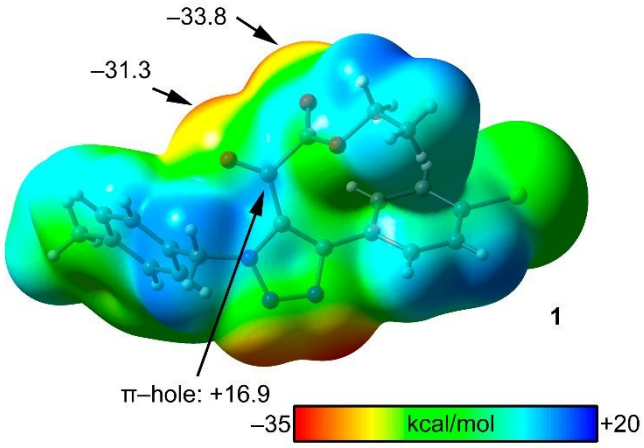

Fig. 8 MEP surface (0.001 a.u. isosurface) at the PBE1PBE-D3/def2-TZVP level of theory of compound **1**. The MEP values at selected points of the surface are indicated in kcal/mol.

Table 3 shows that the MEP values at the O-atoms of the ethyl-2-oxoacetate group are similar in compounds **1**–**3** and more negative in compound **4** likely due to the electron donating methoxy group. In contrast, compound **4** presents the smallest π-hole value and compound **3** (with the electron withdrawing F-atom) presents the most intense π-hole.

Table 3. MEP values in kcal/mol at the C's π–hole and at the O-atoms from keto and carbonyl ester for compounds **1**–**4** at the PBE1PBE/def2-TZVP.

Compound	$V_{s,\pi\text{-hole}}$	$V_{s,O(\text{-CO-})}$	$V_{s,O(COOR)}$
1	+16.9	–32.3	–33.8
2	+12.9	–33.2	–34.5
3	+17.0	–32.6	–33.8
4	+12.5	–35.7	–37.0

In the solid state, compounds **1**–**4** form infinite 1D supramolecular chains (see Fig. 9a for the representative compound **1**) that propagates by means of π–π interactions that interconnect the self-assembled dimers. A detail of the self-assembled dimer is shown in Fig. 9b, where the formation of a hydrogen bonding network is highlighted using green dashed lines. The H-bonds are established between the aromatic H-atoms and the O-atoms of the ethyl-2-oxoacetate group. Moreover, the formation of two symmetrically equivalent O···C interactions is also highlighted using blue dashed lines. The most nucleophilic O-atom belonging to the ester group is located exactly above the electrophilic C-atom of the keto group. The O···C distance is significantly shorter than the sum of van der Waals radii (3.22 Å), thus evidencing the importance of this non-covalent contact.

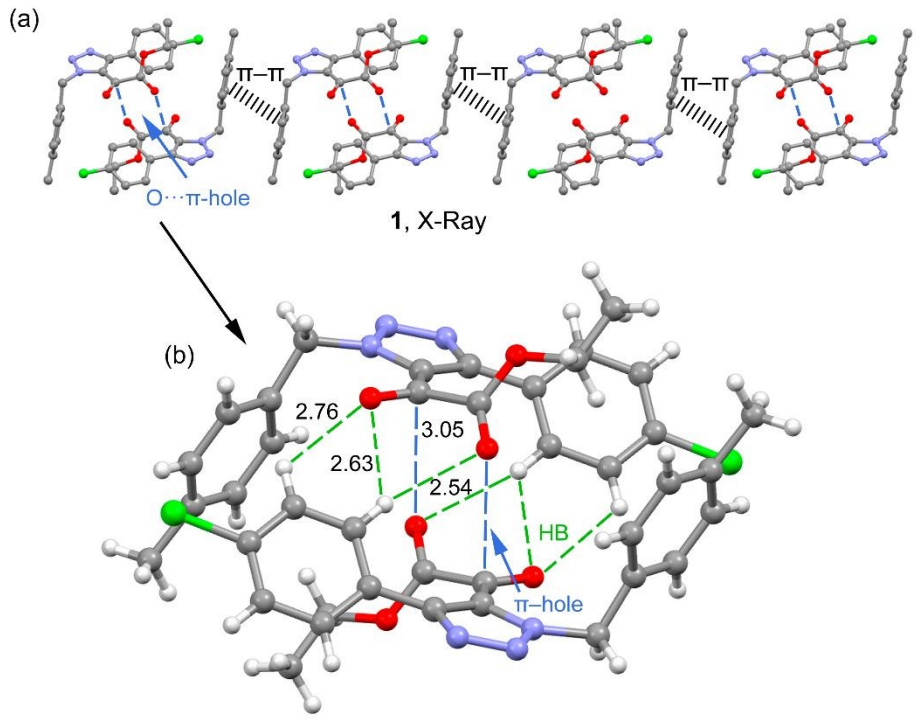

Fig. 9 (a) 1D infinite chain observed in the solid state of compound 1. (b) Detail of the self-assembled dimer. Distances in Å.

We have analyzed the O···C(π-hole) tetrel bonding interactions using DFT calculations. We have first computed the dimerization energies of the dimers of compounds **1**–**4** (see Fig. 10a) and also the dimerization energies of reduced theoretical models (see Fig. 10b) where both phenyl rings have been substituted by H-atoms (see small arrows in Fig. 10b). In these reduced models the H-bonds and other van der Waals interactions due to the

proximity of the bulk of both molecules are not established, and consequently only the contribution of the π–hole tetrel bonding interaction is evaluated. The energetic results along with some geometric features of the complexes are given in Fig. 10 (bottom). The energetic results show that the dimerization energies are very large ranging from –16.0 to –23.2 kcal/mol due to the contribution of both the H-bonds and π–hole interactions. It is interesting to highlight that the O···C π–hole distance is shorter in compound **4** that, conversely, presents the smallest MEP at the π–hole (see Table 3). This fact is compensated by the large and negative value at the O-atom. In fact, this compound presents the largest interaction energy for the reduced model [ΔE(B)] thus confirming that it exhibits the strongest π–hole tetrel bonding interaction. The weakest interaction is observed in compound **2**, that presents the longest O···C distance and also a small MEP value at the π-hole (see Table 3)

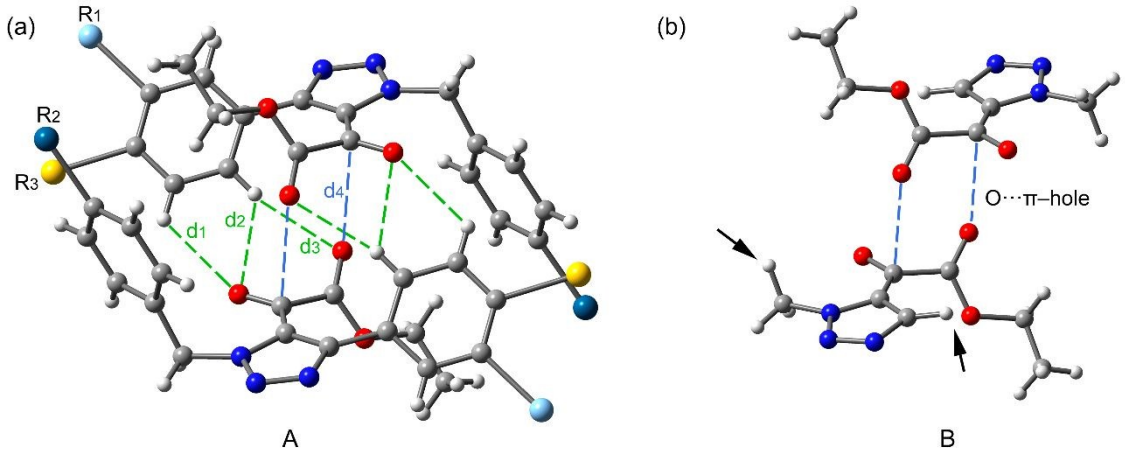

Cmpd	R1	R2	R3	d1	d2	d3	d4	ΔE(A)	ΔE(B)
1	H	CH_3	Cl	2.766	2.637	2.546	3.052	–23.0	–6.5
2	H	CH_3	H	2.905	2.759	2.629	3.172	–16.8	–5.8
3	F	H	H	2.957	2.598	2.539	3.019	–19.4	–7.1
4	H	H	OCH_3	3.021	2.732	2.548	2.905	–23.2	–8.6

Fig. 10 Energetic and geometric features of the self-assembled dimers of compounds **1**–**4** (a) and the reduced model (b). Energies in kcal/mol and distances in Å. The H-bonds are represented using green dashed lines and the O···π–hole interaction using blue dashed lines.

Finally, we have characterized the interactions by using the Bader's quantum theory of "atoms-in-molecules" QTAIM in order to further evidence the existence of the O···π–hole and C–H···O interactions. The presence of a bond path (lines of maximum density linking neighboring nuclei in a system) and bond critical point connecting two atoms is a

universal evidence of interaction[46]. The distribution of bond CPs and bond paths in the dimer of compound **1** as a representative complex is given in Fig. 11. The O···π-hole interaction is characterized by a bond CP (blue sphere) and bond path interconnecting the O and C atoms and confirming the interaction. Each C–H···O interaction (green spheres) is also characterized by a bond CP and bond path that connect the H atom to the O atom of the keto/ester group. The QTAIM analysis also reveals the existence of C–H···π interactions that are formed between the aliphatic H-atom and the electron rich aromatic ring that further contribute to the stabilization of the self-assembled dimers. It is worth emphasizing that the value of charge density ρ(r) at the bond CP is a good indicator of the strength of the interaction, as demonstrated in a great deal of interactions.[47-50] The values of ρ(r) at the bond CPs that characterize the π-hole interactions in complexes **1**–**4** are also included in Fig. 6 along with the dimerization energies of the reduced model complexes. They confirm that the π-hole interaction in **4** is stronger than that in compounds **1**–**3**, also in agreement with the O···C distances (d_4 values in Fig. 11). In fact, we have represented the value of ρ(r) at the bond CP that characterizes the π–hole interaction versus the interaction energies of the model compounds and we have found a very strong linear relationship ($R^2 = 0.9818$), thus confirming that the ρ(r) at the bond CP is a good indicator of the strength of the interaction and also that the reduced model complexes are adequate to analyze the contribution of the π-hole interactions (Fig. 12). Taking into consideration that the ΔE(B) values gathered in Fig. 11 range from –5.8 to –8.6 kcal/mol, each π-hole interaction is energetically significant and comparable to a H-bond interaction.

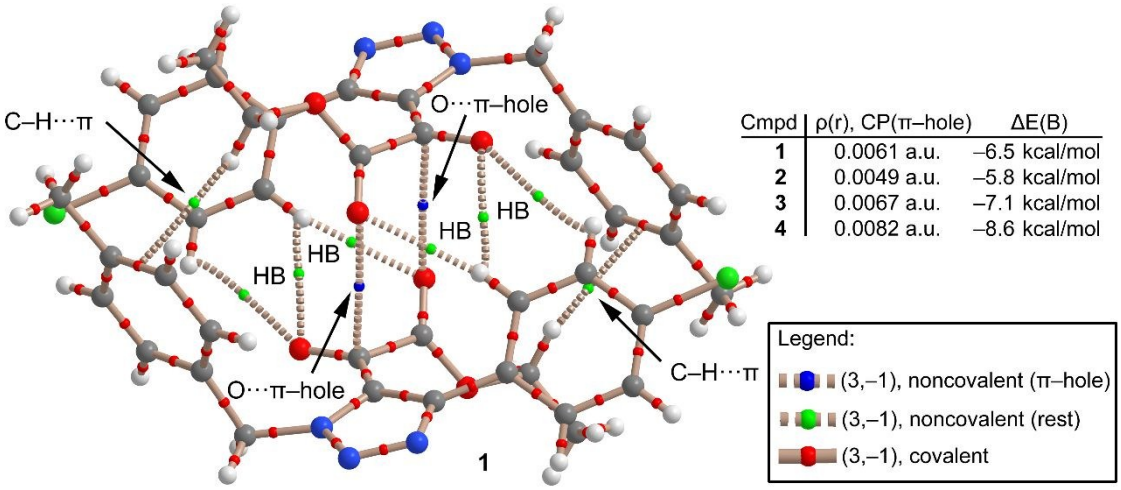

View Article Online
DOI: 10.1039/D0CE00335B

Fig. 11 Distribution of bond critical points and bond paths in complex **1**. ring and cage CPs have been omitted for clarity. Moreover, the bond CPs and bond paths corresponding to intramolecular interactions have been also omitted.

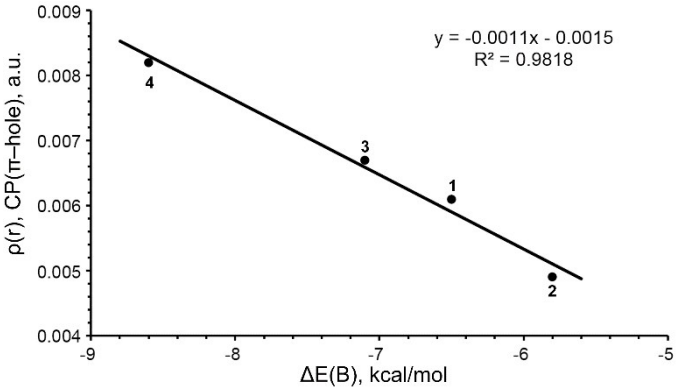

Fig. 12 Regression plot of electron density values [ρ(r)] at the bond CP that characterizes the π–hole interaction versus the interaction energies.

Conclusion

In this work we have synthesized and X-ray characterized four new triazole derivatives those exhibit a strong tendency, *via* the α-ketoester group, to establish two simultaneous π–hole donor-acceptor interactions. The interaction is moderately strong as evidenced by DFT calculations. The O··· π–hole interactions have been characterized by means of Hirshfeld surface analysis, QTAIM and MEP computational tools. The ρ(r) density values at the bond CPs can be used as a measure of the strength of the interaction. The results reported herein are useful empirical principles of π-hole interactions in crystal engineering and supramolecular chemistry, where these interactions are progressively accepted as functionally relevant.

Conflicts of interest

There is no conflict to declare

Acknowledgements

Authors are thankful to the University of Azad Jammu and Kashmir, Muzaffarabad for financial support. Antonio Frontera acknowledges financial support from AEI for the funding of project CTQ2017-85821-R (MICIU/AEI/FEDER, EU)

References

1. J. E. Moses and A. D. Moorhouse, *Chem. Soc. Rev.*, 2007, **36**, 1249-1262.
2. Z. Chen, Z. Liu, G. Cao, H. Li and H. Ren, *Adv. Synth. Catal.*, 2017, **359**, 202-224.
3. D. R. Buckle, C. J. Rockell, H. Smith and B. A. Spicer, *J. Med. Chem.*, 1986, **29**, 2262-2267.
4. I. Oura, K. Shimizu, K. Ogata and S.-i. Fukuzawa, *Org. Lett.*, 2010, **12**, 1752-1755.
5. G. Gilli and P. Gilli, *The nature of the hydrogen bond: outline of a comprehensive hydrogen bond theory*, Oxford University Press, 2009.
6. G. R. Desiraju and T. Steiner, *The weak hydrogen bond: in structural chemistry and biology*, International Union of Crystal, 2001.
7. S. Scheiner, *Hydrogen bonding: a theoretical perspective*, Oxford University Press on Demand, 1997.
8. S. J. Grabowski, *Hydrogen bonding: new insights*, Springer, 2006.
9. P. Politzer and J. S. Murray, in *Noncovalent forces*, Springer, 2015, pp. 291-321.
10. J. S. Murray, P. Lane, T. Clark, K. E. Riley and P. Politzer, *J. Mol. Model.*, 2012, **18**, 541-548.
11. B. L. Schottel, H. T. Chifotides and K. R. Dunbar, *Chem. Soc. Rev.*, 2008, **37**, 68-83.
12. L. Li, Y.-J. Hong, Y. Lin, W.-C. Xiao and M.-J. Lin, *Chem. Commun.*, 2018, **54**, 11941-11944.
13. Y. Chen, J.-J. Liu, C.-R. Fan, J.-Q. Li and M.-J. Lin, *Science China Chemistry*, 2016, **59**, 1492-1497.
14. (a) P. Politzer and J. S. Murray, *J. Comput. Chem.*, 2018, **39**, 464-471; (b) A. Bauzá, T. J. Mooibroek and A. Frontera, *ChemPhysChem*, 2015, **16**, 2496–2517; (c) I. Alkorta, J. Elguero and A. Frontera, *Crystals*, 2020, **10**, 180; (d) A. Bauzá, S. K. Seth and A. Frontera, *Coord. Chem. Rev*., 2019, **384**, 107-125; (e) A. Bauzá and A. Frontera, *Coord. Chem. Rev*., 2020, **404**, 213112; (f) R. M. Gomila and A. Frontera, *CrystEngComm*, 2020, **22**, DOI: 10.1039/D0CE00220H; (g) A. Franconetti and A. Frontera, *Dalton Trans*., 2019, **48**, 11208–11216; (h) S. Mirdya, A. Frontera and S. Chattopadhyay, *CrystEngComm*, 2019, **21**, 6859–6868
15. M. H. Kolar and P. Hobza, *Chem. Rev.*, 2016, **116**, 5155-5187.
16. H. Wang, W. Wang and W. J. Jin, *Chem. Rev.*, 2016, **116**, 5072-5104.
17. R. Sure and S. Grimme, *Chem. Commun.*, 2016, **52**, 9893-9896.
18. P. Politzer, J. S. Murray and T. Clark, *PCCP*, 2013, **15**, 11178-11189.
19. P. Politzer, J. S. Murray and T. Clark, *PCCP*, 2010, **12**, 7748-7757.
20. W. Li, Y. Zeng, X. Li, Z. Sun and L. Meng, *PCCP*, 2016, **18**, 24672-24680.
21. G. J. Bartlett, A. Choudhary, R. T. Raines and D. N. Woolfson, *Nature Chem. Bio.*, 2010, **6**, 615.
22. R. Prohens, D. de Sande, M. Font-Bardia, A. Franconetti, J. F. González and A. Frontera, *Cryst Growth Des.*, 2019, **19**, 3989– 3997
23. A. Bauzá, A. Frontera and T. J. Mooibroek, *Cryst. Growth Des.*, 2016, **16**, 5520-5524.
24. (a) A. Bauzá, A. V. Sharko, G. A. Senchyk, E. B. Rusanov, A. Frontera and K. V. Domasevitch, *CrystEngComm*, 2017, **19**, 1933-1937; (b) A. Franconetti, A. Frontera, T. J. Mooibroek, *CrystEngComm*, 2019, **21**, 5410-5417; (c) B. Galmés, A. Franconetti, A. Frontera, *Int. J. Mol. Sci*., 2019, **20**, 3440
25. A. Bauzá, A. Frontera and T. J. Mooibroek, *Nat. Comm.*, 2017, **8**, 14522.
26. T. J. Mooibroek, *CrystEngComm*, 2017, **19**, 4485-4488.
27. E. C. Escudero-Adán, A. Bauzá, C. Lecomte, A. Frontera and P. Ballester, *PCCP*, 2018, **20**, 24192-24200.
28. S. Grabowski, *Molecules*, 2015, **20**, 11297-11316.
29. S. J. Grabowski, *J. Comput. Chem.*, 2018, **39**, 472-480.
30. D. Dutta, H. Nath, A. Frontera and M. K. Bhattacharyya, *Inorg. Chim. Acta*, 2019, **487**, 354-361.
31. M. N. Ahmed, M. Arif, F. Jabeen, H. A. Khan, K. A. Yasin, M. N. Tahir, A. Franconetti and A. Frontera, *New J. Chem.*, 2019, **43**, 8122-8131.

32. B. Wang, M. N. Ahmed, J. Zhang, W. Chen, X. Wang and Y. Hu, *Tetrahedron Lett.*, 2013, **54**, 6097-6100.
33. M. N. Ahmed, K. A. Yasin, K. Ayub, T. Mahmood, M. N. Tahir, B. A. Khan, M. Hafeez and M. Ahmed, *J. Mol. Struct.*, 2016, **1106**, 430-439.
34. G. M. Sheldrick, SHELXS97 and SHELXL97. Program for Crystal Structure Solution and Refinement. University of Göttingen, Göttingen..
35. G. M. Sheldrick, *Acta Crystal.*, 2015, C**71**, 3-8.
36. H. Andleeb, I. Khan, A. Bauzá, M. N. Tahir, J. Simpson, S. Hameed and A. Frontera, *Acta Cryst.*, 2018, C**74**, 816-829
37. Gaussian 16, Revision A.01, M. J. Frisch, G. W. Trucks, H. B. Schlegel, G. E. Scuseria, M. A. Robb, J. R. Cheeseman, G. Scalmani, V. Barone, G. A. Petersson, H. Nakatsuji, X. Li, M. Caricato, A. V. Marenich, J. Bloino, B. G. Janesko, R. Gomperts, B. Mennucci, H. P. Hratchian, J. V. Ortiz, A. F. Izmaylov, J. L. Sonnenberg, D. Williams-Young, F. Ding, F. Lipparini, F. Egidi, J. Goings, B. Peng, A. Petrone, T. Henderson, D. Ranasinghe, V. G. Zakrzewski, J. Gao, N. Rega, G. Zheng, W. Liang, M. Hada, M. Ehara, K. Toyota, R. Fukuda, J. Hasegawa, M. Ishida, T. Nakajima, Y. Honda, O. Kitao, H. Nakai, T. Vreven, K. Throssell, J. A. Montgomery, Jr., J. E. Peralta, F. Ogliaro, M. J. Bearpark, J. J. Heyd, E. N. Brothers, K. N. Kudin, V. N. Staroverov, T. A. Keith, R. Kobayashi, J. Normand, K. Raghavachari, A. P. Rendell, J. C. Burant, S. S. Iyengar, J. Tomasi, M. Cossi, J. M. Millam, M. Klene, C. Adamo, R. Cammi, J. W. Ochterski, R. L. Martin, K. Morokuma, O. Farkas, J. B. Foresman, and D. J. Fox, Gaussian, Inc., Wallingford CT, 2016
38. S. Grimme, J. Antony, S. Ehrlich and H. Krieg, *J. Chem. Phys.*, 2010, **132**, 154104.
39. S. M. Nashre-ul-Islam, D. Dutta, P. Sharma, A. K. Verma, A. Frontera and M. K. Bhattacharyya, *Inorg. Chim. Acta*, 2019, **498**, 119108.
40. R. F. Bader, *Chem. Rev.*, 1991, **91**, 893-928.
41. K. T. AIMAll, *Overland Park KS, USA,(aim. tkgristmill. com)*, 2016.
42. J. J. McKinnon, M. A. Spackman and A. S. Mitchell, *Acta Cryst.*, 2004, **B60**, 627-668.
43. J. J. McKinnon, D. Jayatilaka and M. A. Spackman, *Chem. Commun.*, 2007, 3814-3816.
44. M. A. Spackman and D. Jayatilaka, *CrystEngComm*, 2009, **11**, 19-32.
45. S. Wolff, D. Grimwood, J. McKinnon, M. Turner, D. Jayatilaka and M. Spackman, *University of Western Australia*, 2012.
46. R. F. Bader, *J. Phys. Chem. A*, 1998, **102**, 7314-7323.
47. E. Cubero, M. Orozco and F. Luque, *J. Phys. Chem. A* , 1999, **103**, 315-321.
48. C. Garau, A. Frontera, D. Quiñonero, P. Ballester, A. Costa and P. M. Deyà, *ChemPhysChem*, 2003, **4**, 1344-1348.
49. (a) Y. Roselló, M. Benito, E. Molins, M. Barceló-Oliver and A. Frontera, *Crystals*, 2019, **9**, 224; (b) M. Mirzaei, F. Sadeghi, K. Molčanov, J. K. Zaręba, R. M. Gomila and A. Frontera, *Cryst. Growth Des*. 2020, **20**, 1738-1751; (c)
50. (a) B. Galmés, D. Martínez, M. F. Infante-Carrió, A. Franconetti and A. Frontera, *ChemPhysChem*, 2019, **20**, 1135-1144; (b) A. Bauza and A. Frontera, *ChemPhysChem*, 2020, **21**, 26-3.

In this manuscript we report the synthesis and X-Ray characterization of four triazole derivatives that include an α-ketoester functionality and two phenyl substituents. These compounds form self-assembled dimers in the solid state establishing two symmetrically equivalent O··· π-hole interactions.

View Article Online
DOI: 10.1039/D0CE00335B